ADVANCED MATERIALS INTERFACES
www.advmatinterfaces.de

Strategies for Analyzing Noncommon-Atom Heterovalent Interfaces: The Case of CdTe-on-InSb

Esperanza Luna, Achim Trampert, Jing Lu, Toshihiro Aoki, Yong-Hang Zhang, Martha R. McCartney, and David J. Smith*

Semiconductor heterostructures are intrinsic to a wide range of modern-day electronic devices, such as computers, light-emitting devices, and photodetectors. Knowledge of chemical interfacial profiles in these structures is critical to the task of optimizing the device performance. This work presents an analysis of the composition profile and strain across the noncommon-atom heterovalent CdTe/InSb interface, carried out using a combination of electron microscopy imaging techniques. Because of the close atomic numbers of the constituent elements, techniques such as high-angle annular-dark-field and large-angle bright-field scanning transmission electron microscopy, as well as electron energy-loss spectroscopy, give results from the interface region that are inherently difficult to interpret. By contrast, use of the 002 dark-field imaging technique emphasizes the interface location by comparing differences in structure factors between the two materials. Comparisons of experimental and simulated CdTe-on-InSb profiles reveal that the interface is structurally abrupt to within about 1.5 nm (10–90% criterion), while geometric phase analysis based on aberration-corrected electron microscopy images reveals a minimal level of interfacial strain. The present investigation opens new routes to the systematic investigation of heterovalent interfaces, formed by the combination of other valence-mismatched material systems.

1. Introduction

The selective combination of closely lattice-matched group II–VI/group III–V compound semiconductors offers many potential benefits due to the wide range of bandgap energies achievable,[1] as well as novel electronic effects at the interface arising from the valence mismatch. The presence of novel transport properties with high interfacial sheet charge,[2] a range of band offsets associated with local interfacial dipoles,[3] and possible transitions to new topological insulators[4] are anticipated. The appearance and effectiveness of such effects are crucially dependent on the character of the noncommon-atom (NCA) interface, i.e., whether a sharp polar interface is formed or, on the contrary, if there are mixtures of chemical bonds across the interface (II–V or III–VI bonds) leading to a nonpolar interface, which is otherwise the predicted energetically stable configuration.[5–7] Very little has so far been done to exploit these opportunities, in part due to challenges in determining the structure and properties of these types of interface, for example, by using scanning transmission electron microscopy (STEM) techniques. Recent advances in aberration-corrected (AC) electron microscopy have enabled information limits well beyond the 1 Å to be obtained, and it has become straightforward to resolve projections of individual atomic columns making it possible, in principle, to determine atomic arrangements at the interface.[8] There are, however, intrinsic limitations in the interpretation of images from the heterointerface, depending on the material combination under consideration. One such challenge is the CdTe-on-InSb interface, a heterostructure with renewed interest due to its potentially novel functionalities.[4]

Dr. E. Luna, Dr. A. Trampert
Paul-Drude-Institut für Festkörperelektronik
Leibniz-Institut im Forschungsverbund Berlin e.V
Hausvogteiplatz 5-7, D-10117 Berlin, Germany
E-mail: luna@pdi-berlin.de
Dr. J. Lu
School of Engineering for Matter
Transport and Energy
Arizona State University
Tempe, AZ 85287, USA
The ORCID identification number(s) for the author(s) of this article can be found under https://doi.org/10.1002/admi.201901658.

DOI: 10.1002/admi.201901658

Dr. T. Aoki
LeRoy Eyring Center for Solid State Science
Arizona State University
Tempe, AZ 85287, USA
Prof. Y.-H. Zhang
School of Electrical, Computer and Energy Engineering
Arizona State University
Tempe, AZ 85287, USA
Prof. M. R. McCartney, Prof. D. J. Smith
Department of Physics
Arizona State University
Tempe, AZ 85287, USA

There has been a long tradition in the study of epitaxial CdTe films and related heterostructures grown by molecular beam epitaxy (MBE), in part because of their well-known applications in optoelectronic devices (e.g., infrared photodetectors, solar cells), as well as the possibility of providing buffer layers for the growth of HgCdTe alloys on commonly available substrates.[1] Recent works demonstrate that CdTe is an excellent material for solar cell applications, where significant improvements in the material quality lead to device performance records that place this material well beyond previous limits.[9,10] A key factor in the successful CdTe growth was the introduction of an InSb buffer layer before CdTe growth. The use of InSb as a candidate substrate for the CdTe growth appears close to ideal because the two materials are nearly lattice-matched (a_{InSb} = 6.479 Å, a_{CdTe} = 6.482 Å at room temperature) and they have similar thermal expansion coefficients.[11] Epitaxial growth of CdTe on (almost) lattice-matched InSb substrates should thus provide a viable path toward achieving very high quality material, although unanswered questions still remain about the interfacial region.

The combination of CdTe (II−VI) and InSb (III−V) implies the existence of a heterovalent NCA interface, i.e., the interface must contain mixtures of II−V and/or III−VI bonds due to the valence mismatch between the two materials. Moreover, the close proximity in atomic numbers of the four elements Cd (Z = 48), In (Z = 49), Sb (Z = 51), and Te (Z = 52) at the CdTe/InSb interface, will make it difficult to reliably identify the individual species based on image intensity differences, even though the projected atomic columns can be readily resolved with the latest generation of AC-STEMs.[12] Compositional analysis using either electron-energy-loss spectroscopy (EELS) or energy-dispersive X-ray spectroscopy (EDS) is also challenging because the close atomic numbers of the constituent elements result in overlapping spectral features that are difficult to separate and interpret quantitatively. Hence, details about the interface stoichiometry or the composition profile remain unclear. The ideal electron microscopy approach would be to combine different (S)TEM techniques that probe the interface on different length scales to uncover all relevant features. A method that allows quantification of the interface stoichiometry, providing information that is complementary to that available from atomically resolved AC-STEM, EELS, and EDS, is thus highly desirable.

A procedure based on conventional TEM has been previously developed that enabled reliable and systematic quantification of interfacial intermixing, i.e., the composition profile, across isovalent NCA interfaces.[13] This approach permits detection of variations in the interface width that are smaller than the resolution of the $\mathbf{g}_{002}$ dark-field (DF) TEM technique used for imaging (about 0.5 nm). As shown in this present work, the method is of more general applicability, since it can be successfully applied to the case of heterovalent CdTe/InSb NCA interfaces where it enables reliable identification of the interface position, determination of the composition profile, and, in particular, quantification of the chemical width. The experimental results demonstrate that the CdTe-on-InSb chemical interface is very narrow, extending over ≈1.5 nm only (10–90% criterion), and chemically mixed. This value is on the same order as the chemical interface profile measured in the InAs/GaSb NCA system (1.3 nm),[13,14] and is remarkably smaller than the interfacial intermixing observed in other isovalent common-atom III−V heterointerfaces, e.g., 2.1 nm for high quality (Al,Ga)As/GaAs.[14]

2. Results

2.1. (S)TEM Investigation of CdTe/InSb: Interface Roughness

The properties and behavior of layered materials depend strongly on the atomic-scale structural interface roughness (i.e., steps and islands) and on any chemical mixing across the interface.[15] Investigation of interfacial roughness using different (S)TEM techniques indicates coherent, defect-free CdTe/InSb interfaces, as shown in **Figure 1**, which displays several (S)TEM images, each probing the interface on different length scales ranging from the hundreds of nanometer scale of conventional DFTEM images to the atomically resolved AC-STEM image, which resolves projections of individual atomic columns, commonly called "dumbbells."[8]

Quantitative analysis of intensity profiles was carried out on pairs of high-angle annular-dark-field (HAADF) and large-angle bright-field (LABF) images that were recorded simultaneously in order to identify the interface position by measuring its width and the atom termination. These two imaging modes are closely related since they both provide incoherent, Z-dependent image contrast with no contrast inversions with changes in objective lens defocus or sample thickness.[12] The reduced Z dependence of LABF images means that this imaging mode is preferred for studying compound semiconductors with widely differing Z, whereas HAADF images are preferable when the elements have quite similar Z, which is the case for Cd (48), Te (52)/In (49), Sb (51). Thus, **Figure 2**a shows an aberration-corrected HAADF STEM image across the CdTe/InSb interface, and Figure 2b reveals an intensity profile after summing over 11 separate rows of atomic columns to improve the signal-to-noise ratio. Clear intensity differences are apparent for the atomic columns within each dumbbell pair, and it is possible to identify the dumbbell polarity with the heavier anion Sb to the left of each pair of atomic columns on the left side of the interface, and the heavier anion Te to the left of each pair on the right side of the interface, as indicated in Figure 2a. Significantly, the exact interface position cannot be determined unambiguously, because there is no notable measurable difference in the dumbbell spacing across the interface. Furthermore, the intensity variations of the dumbbells do not remarkably change, which can be attributed to chemical intermixing between In and Cd and, on the other hand, between Sb and Te. By contrast, use of the chemically sensitive $\mathbf{g}_{002}$ DFTEM imaging technique emphasizes the interface location by comparing differences in structure factors between the two materials, as clearly visible in Figure 1c. Furthermore, the composition profile across the interface can be inferred from the analysis of the intensity of the $\mathbf{g}_{002}$ DFTEM images (cf. Figure 1d), as extensively presented in Section 2.3.

The aberration-corrected STEM images of the CdTe/InSb interface region were analyzed further to assess the presence and extent of any interfacial strain using the geometric phase analysis (GPA) technique.[16] Basically, this technique enables an assessment to be made of any local lattice strain using a neighboring strain-free region as a reference for the analysis. Since the out-of-plane strain was of primary interest in these observations, images were recorded with the interface normal aligned to be horizontal so that the effect of any scanning distortions would be minimized. The representative HAADF STEM image shown in Figure 2a reveals that the individual pairs of atomic columns of Cd and Te, and In and Sb, are well resolved, and there are no

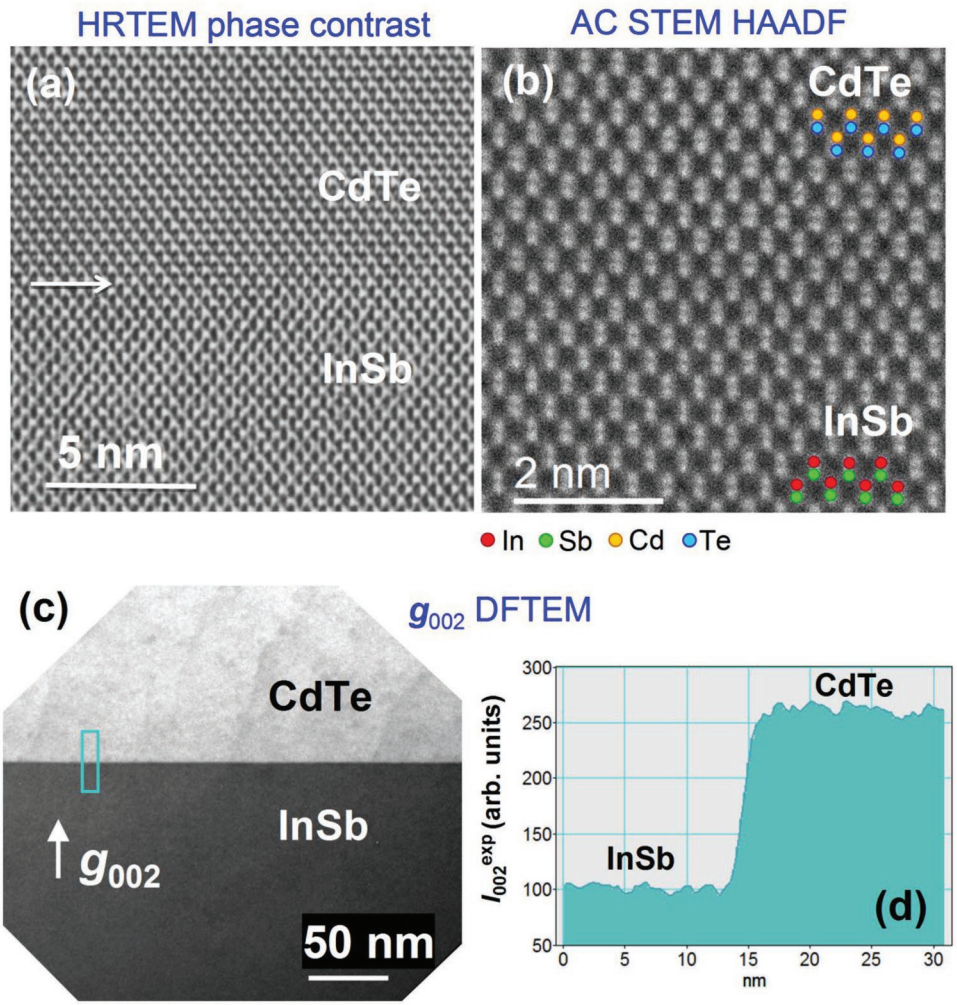

Figure 1. Cross-sections of CdTe/InSb heterostructure recorded in several different TEM imaging modes: a) high-resolution (HR), phase-contrast TEM image; b) aberration-corrected, high-angle annular-dark-field (HAADF) STEM image; and c) 002 DFTEM image together with d) intensity line profile at the CdTe/InSb interface.

indications of any interfacial defects. Figure 2c shows the corresponding Fast Fourier Transform calculated from Figure 2a. The circled 400 and 2–20 spots were then used to generate the out-of-plane strain map shown in Figure 2d, with a spatial resolution of ≈1nm, as determined by the effective aperture size applied in reciprocal space when processing was done. The strain map appears to be relatively uniform across the entire field of view except for a narrow region near the interface at the top of the field of view, and does not suggest the presence of any rigid-body displacement at the interface, as we had reported in an earlier study.[17] Thus, it is concluded based on our present GPA analysis that the CdTe/InSb interface is effectively strain-free to within the measurement limits of the GPA technique.

2.2. Interfacial Intermixing at Isovalent NCA Interfaces: Methodology

The interfacial intermixing generally superimposes on the interfacial roughness. Since the intermixing is commonly larger (on the nanometer scale) than the interfacial roughness (on the atomic scale), the major contribution to the more general interface width is determined by the continuous change in composition across the interface, i.e., by the chemical mixing. The composition profile across isovalent common-atom interfaces can be directly inferred from analysis of the intensity of the chemically sensitive $\mathbf{g}_{002}$ DFTEM images, following the procedures developed previously.[18,19] The motivation for this approach is that the diffracted intensity for 002 reflection[18] under a kinematic approximation for compound semiconductors with zincblende structure, is proportional to the square of the structure factor, which in turn depends on the difference in the atomic scattering factors f of the separate alloy components. Thus, in this "structure-factor imaging mode," the image contrast arises primarily from differences in the atomic-scattering factors between the group-III and group-V elements of III−V compounds (or the group-II and group-VI elements of II−VI compounds). This direct procedure, however, cannot be simply applied to NCA interfaces due to the lack of a common atom across the interfaces.

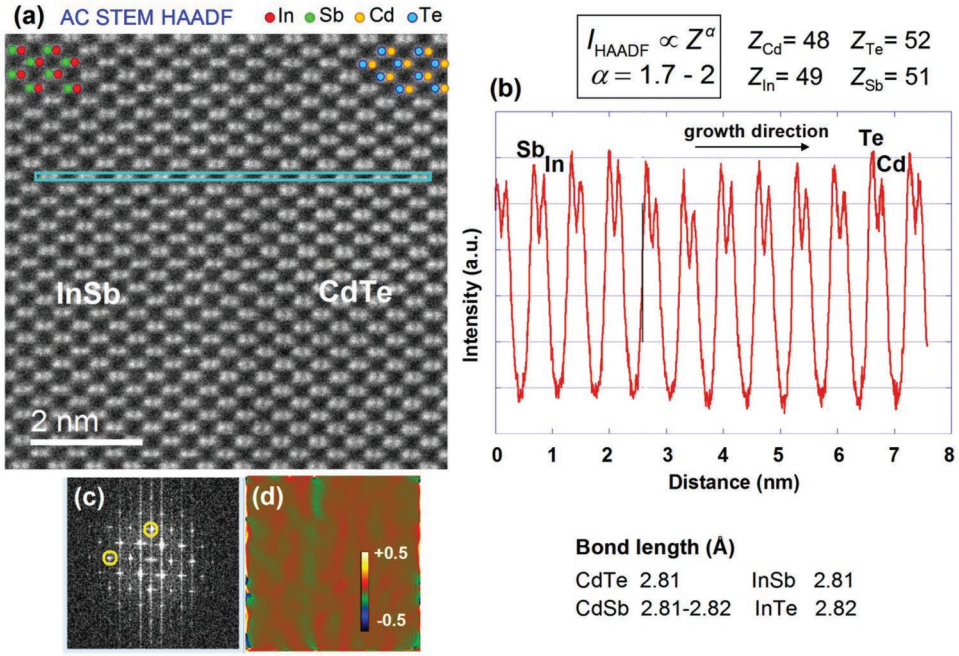

Figure 2. a) HAADF image of CdTe/InSb interface. b) Intensity profile from HAADF image summed over 11 rows of atomic columns. Geometric Phase Analysis of heterovalent CdTe/InSb interface: c) the corresponding FFT as applied to (a), and d) strain map calculated using 400 and 2–20 Bragg spots with spatial resolution of 1 nm, as determined by aperture size used during processing.

A methodology has been developed for reliable and systematic characterization of isovalent NCA interfaces.[13] The method, originally applied to the investigation of InAs/GaSb interfaces, relies on analysis of the intensity (i.e., I_{002}^{exp}) in $\mathbf{g}_{002}$ DFTEM images. The method is based on the insertion of a proposed distribution profile for the different constituent elements into a calculation of the corresponding diffracted intensity under kinematic conditions I_{002}^{sim}. The simulated intensity I_{002}^{sim} is compared with the experimental I_{002}^{exp}, while searching for the composition profiles that fit best with the experimental image contrast.[13,20] In order to avoid measuring absolute intensities, the scattered intensities of the layers are normalized to that of a reference layer of known composition with the same thickness, $R_{002} = I_{002}^{layer}/I_{002}^{ref.}$. Thus, the analysis basically relies on comparison of experimental R_{002}^{exp} and simulated R_{002}^{sim} curves. The procedure resembles the standard analysis of X-ray diffraction data where the layer information (composition, thickness, strain, etc.) is extracted after comparing experimental and simulated curves.

The key issue here is identification of the elemental distribution profile. From analysis of directly determined experimental composition profiles across isovalent common-atom interfaces [e.g., (Al,Ga)As/GaAs, (In,Ga)As/GaAs], it has previously been demonstrated that the smooth variation of element concentration x with position z across the interface follows a sigmoidal law, $x(z) = x_0/[1 + \exp(-z/L)]$ with the interface width, L, as the main fitting parameter,[13,19,20] and x_0 is the nominal mole fraction. The parameter L quantifies the interface width, which is proportional to the length W over which the concentration changes from 10% to 90% of its plateau value, $W = 4.4L$.[13,19,20] Such functional dependence for the transition region (i.e., the sigmoidal profile) arises from fundamental growth processes during the interface formation.[14] Indeed, nonvanishing interface broadening is predicted for any semiconductor heterointerface, which will always be characterized by an intrinsic minimum width that is dictated by the molecule–surface interaction potential during growth.[14] In the specific case of the InAs/GaSb NCA structure, assuming formation of the quaternary $In_xGa_{1-x}As_ySb_{1-y}$ alloy at the interface, realistic distributions for In and As are obtained assuming that both the In and As distributions follow the sigmoidal profile (and those for Ga and Sb are then obtained using mass conservation, [In] + [Ga] = 100% and [As] + [Sb] = 100%). These distributions are used as input for the calculation of $I_{002}^{sim}(R_{002}^{sim})$. Since the identities of both the cation and the anion change across the heterointerface, the separate contributions of the III- and V-elements need to be inserted separately. Thus, the group-III (In—Ga) and group-V (As—Sb) intermixing are independently determined.

2.3. Interfacial Intermixing at Heterovalent NCA Interfaces: Proposed Methodology

An extension of the approach described above is proposed here in order to systematically evaluate the extent of interfacial mixing across the heterovalent CdTe/InSb NCA interface. Since both CdTe and InSb compounds have the zincblende structure, then $\mathbf{g}_{002}$ DFTEM images still retain their chemical-sensitive character, as clearly evident from the contrast difference visible in Figure 1c, where the structure factors of CdTe and InSb serve to emphasize the interface location. Nevertheless, in order to extract quantitative information from the DFTEM images, several assumptions need to be made. As done previously for InAs/GaSb where the interface consisted of (In,Ga)(As,Sb),[13] the formation of quaternary InSbCdTe alloys at the interface is

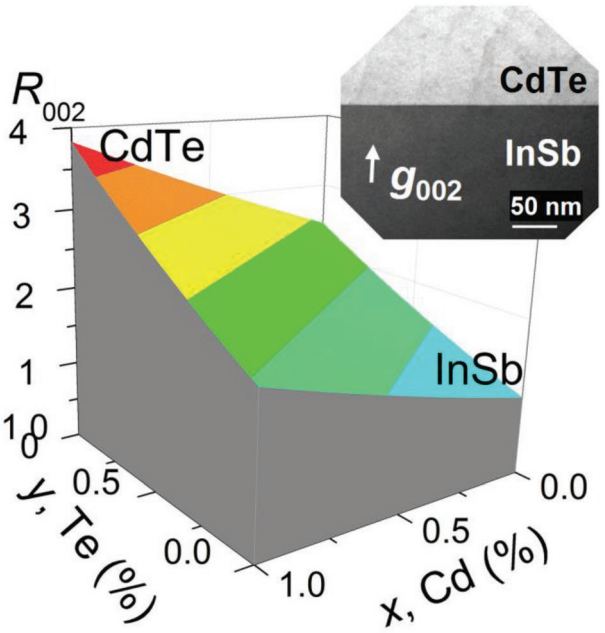

Figure 3. Plot showing variation of $\mathbf{g}_{002}$ DFTEM relative image intensity as a function of Cd% (*x*-axis) and Te% (*y*-axis). Note almost linear dependence on both *x* and *y*.

postulated. Furthermore, it is assumed that the quaternary can be expressed as $In_{1-x}Sb_{1-y}Cd_xTe_y$, where the group-II element Cd would behave like a group-III element and bond with the group-V element Sb (leading to II—V bonds), and the group-VI element Te would behave like a group-V element and bond with the group-III element In (giving rise to III—VI bonds). Moreover, mean group-III-II atomic scattering factor f_{III_II} and mean group-V-VI atomic scattering factor f_{V_VI}, are defined, and it is assumed that the elemental mixing follows a linear dependence (similar to Vegard's law) so that $f_{III\_II} = xf_{II} + (1–x)f_{III}$ and $f_{V\_VI} = yf_{VI} + (1 - y)f_V$. The calculation uses the atomic scattering factors f_{Cd}, f_{In}, and f_{Sb} given by Doyle and Turner (DT).[21] Since no data for f_{Te} are available from DT, f_{Te} is estimated using the Peng–Ren–Dudarev–Whelan (PRDW) parameterization.[22] Previously, it was confirmed that DT and PRDW yielded identical values for f_{Cd}, f_{In}, and f_{Sb}. In the computations, the parameters are inserted as directly extracted from the original papers,[21,22] and then a cross-check is made that the estimated *f* values agree with those deduced using the simulation program JEMS.[23]

Substitution, taking the InSb layer as reference of known composition, gives the dependence $R_{002} = I_{002}/I_{002}^{InSb} = (1 + Ax + By)^2$ where $A = (f_{Cd} - f_{In})/(f_{In} - f_{Sb})$ and $B = (f_{Sb} - f_{Te})/(f_{In} - f_{Sb})$. The plot of R_{002} as a function of *x* (Cd%) and *y* (Te%) is presented in **Figure 3**, and predicts brighter contrast for the CdTe layer, in agreement with experimental observations (cf. Figure 1c and inset in Figure 3). Theory also predicts that the ratio between the diffracted intensity in the separate CdTe and InSb layers is given as $R_{002}(I_{002}^{CdTe}/I_{002}^{InSb}) = 3.83$. However, the ratio obtained from the experimental images shows a slight but systematic deviation from the theoretical value, with $R_{002}^{exp} \approx 3.6–3.78$, which is possibly due to some contribution from inelastic electron scattering.[24] Hence, the experimental intensity profiles R_{002}^{exp} are initially calibrated and normalized to $R_{002}(I_{002}^{CdTe}/I_{002}^{InSb}) = 3.83$.

The iterative procedure used to determine the composition profiles across the CdTe/InSb interfaces is displayed in **Figure 4** and can be summarized as follows. First, a realistic composition profile is proposed for Cd and Te, each based on a sigmoidal function, see Figure 4b (and those for In and Sb are based on [In] + [Cd] = 100% and [Sb] + [Te] = 100%, assuming the formation of $In_{1-x}Sb_{1-y}Cd_xTe_y$ at the interface). As for the isovalent NCA case, each profile, i.e., Cd and Te, is independently inserted into the calculation. The simulated diffracted intensity ratio R_{002} is then calculated and compared with the experimental R_{002}^{exp} profile (Figure 4c). When the match between R_{002} and R_{002}^{exp} is judged as unsatisfactory, new profiles for Cd and Te are inserted into the calculation. The process is iterated until the best fitting between R_{002} and R_{002}^{exp} is reached.

This analysis is applied to two different InSb/CdTe heterostructures having the same nominal growth conditions.

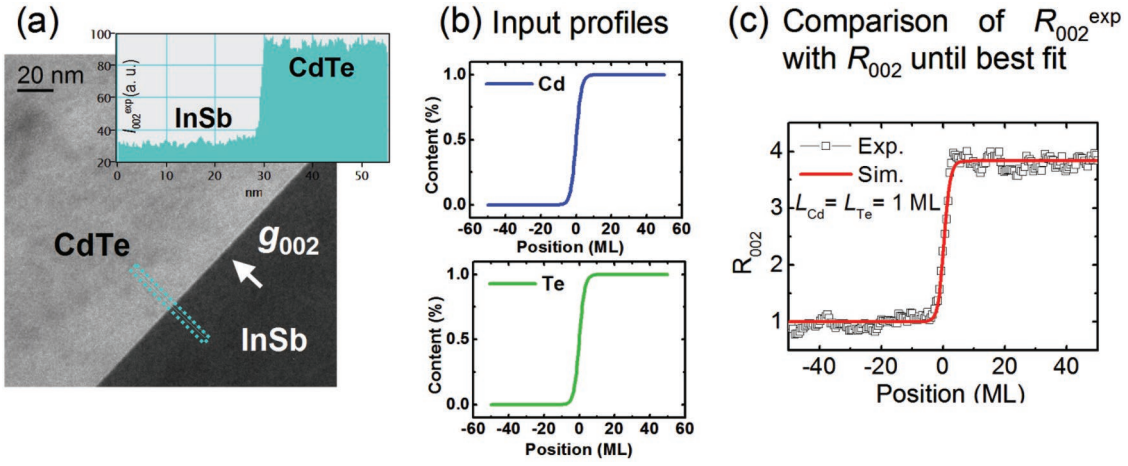

Figure 4. Schematic representation of the iterative procedure used to determine the composition profiles across the heterovalent CdTe/InSb NCA interface. a) Chemically sensitive 002 DFTEM image. Inset shows I_{002}^{exp} intensity line scan used to evaluate the ratio R_{002}^{exp} $(I_{002}^{CdTe}/I_{002}^{InSb})$. b) Composition profiles for Cd and Te, each based on sigmoidal functions, used as input for the calculation of R_{002} $(I_{002}^{CdTe}/I_{002}^{InSb})$. c) Comparison made with R_{002}^{exp} until best fit obtained.

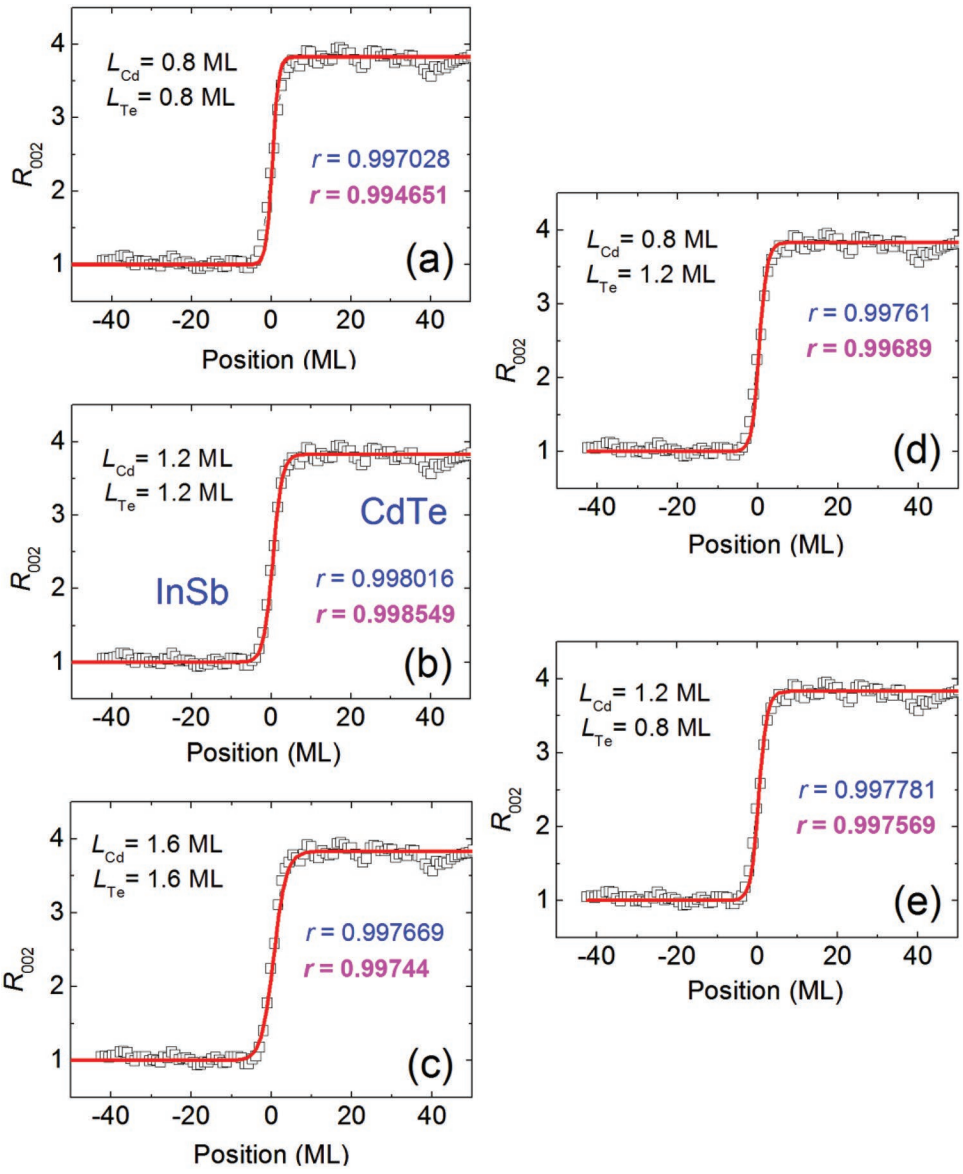

Figure 5. Series of plots showing comparisons between experimental intensity profiles (shown as small squares) with simulated profiles based on different elemental profiles as quantified by different values of interface parameter *L* indicated on each plot: a) $L_{Cd,Te}$ = 0.8 monolayers (ML); b) $L_{Cd,Te}$ = 1.2 ML (best fit); c) $L_{Cd,Te}$ = 1.6 ML; d) L_{Cd} = 0.8 ML and L_{Te} = 1.2 ML; and e) L_{Cd} = 1.2 ML and L_{Te} = 0.8 ML. *r* indicates the correlation coefficient for the complete set of data (blue) and for the data at the interface region (bold pink). The data correspond to Sample A.

Figure 5a–e represents a set of experimental (open squares) and simulated curves (continuous lines) that illustrate the effect of changing the interface profile, as characterized by the *L* value. The data correspond to one of the two investigated samples (Sample A). In this particular case, the best fit is obtained for a *L* parameter of $L_{Cd} = L_{Te}$ = 1.2 ML. Note the remarkable good match between R_{002} and R_{002}^{exp} for the profile in Figure 5b, corresponding to the best fit as confirmed by the correlation coefficient *r*. Two correlation coefficients are considered, one for the set of data of the complete profile and another one for the set of data around the interface region between –11.5 and 11.5 ML. A variation in the value of *L* of ±0.4 ML results in obvious discrepancies between R_{002} and R_{002}^{exp}, as displayed in Figure 5a,c. Different L_{Cd} and L_{Te} can be inserted into the calculation, as shown in Figure 5d,e. The best fit, however, is obtained when the two sublattices have a similar interfacial mixing with $L_{Cd} = L_{Te}$. Similar results are obtained for the second sample, Sample B. In this case, the best fit is obtained for an interface parameter $L_{Cd} = L_{Te}$ = 1 ML (given in Figure 4c).

Further analysis indicates that the method can detect variations in the *L* parameter as small as 0.1 ML, as shown in **Figure 6**a,c. This feature is illustrated in Figure 6d which displays the correlation coefficient between the simulated and experimental curves for a series of profiles where $L_{Cd} = L_{Te}$ have been varied between 0.5 and 2 ML. Two correlation coefficients are again considered, following the above definition. The presented data correspond to the second sample investigated in this work, Sample B, where the best fit is obtained for

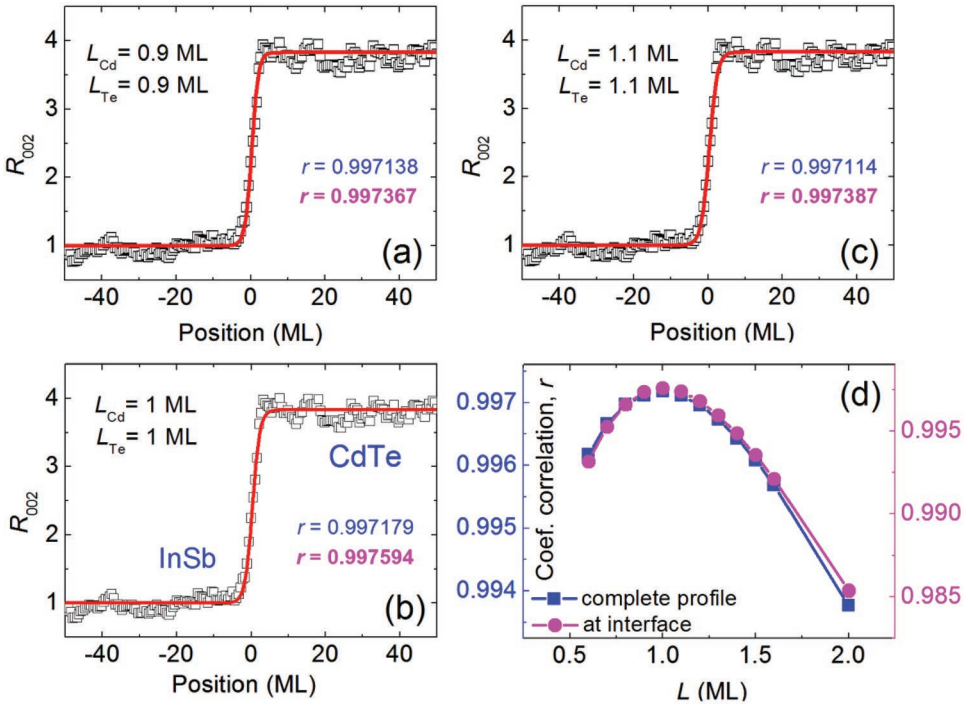

Figure 6. Series of plots showing comparisons between experimental intensity profiles (shown as small squares) with simulated profiles based on different elemental profiles with a variation in the value of the interface parameter L of ±0.1 ML indicated on each plot: a) $L_{Cd,Te}$ = 0.9 ML; b) $L_{Cd,Te}$ = 1 ML (best fit); and c) $L_{Cd,Te}$ = 1.1 ML. r indicates the correlation coefficient for the complete set of data (blue) and for the data at the interface region (bold pink). d) Correlation coefficient plotted as a function of interface width L. The data correspond to Sample B, with the same nominal growth conditions as Sample A.

$L_{Cd} = L_{Te}$ = 1 ML. The plot of the correlation coefficient versus L in Figure 6d clearly shows that: i) the interface width L can be unambiguously determined since there is a well-defined maximum, and ii) variations in abruptness of the interface profile of only 0.1 ML are clearly discernable. Taking into consideration the L values obtained from analysis of the two samples, it is concluded that the CdTe-on-InSb interface is chemically abrupt, extending over ≈1.5 nm (10–90% criterion) with $L_{Cd,Te}$ ≈ 1.1 ML (i.e., averaged L from the two samples). This value is on the same order as the chemical width (1.3 nm) estimated for the InAs/GaSb NCA system measured previously using the same 002 DFTEM imaging approach.[13,14,20] Remarkably, this value is considerably smaller than the interfacial intermixing determined for other isovalent common-atom III−V heterointerfaces, as for instance, 2.1 nm for high quality (Al,Ga)As/GaAs.[14] Moreover, prior estimates of the CdTe-on-InSb interface width had indicated an interface that was locally sharp on the scale of 2 nm.[25] However, this interface evaluation was performed on early CdTe/InSb multilayer structures and there have since been significant advances in both the understanding of growth mechanisms,[26] as well as significant technical developments for MBE growth of combined III−V/II−VI structures.[11]

3. Discussion and Conclusions

Electron microscopy allows materials characterization over a wide range of magnification, with spatial resolution at the atomic scale being routinely achieved with aberration-corrected instruments. Yet, the current study reveals that analysis of the $\mathbf{g}_{002}$ DFTEM intensity profiles as presented here, although based on the resolution-limited DFTEM technique, is far better suited to the specific task of extracting a quantitative estimate of the elemental profile across the CdTe/InSb interface where all of the elements involved have quite similar atomic numbers. The approach does not so far deconvolve the smearing effect of the finite objective size on the profile measurements, which would lead to an overestimate of the interfacial broadening being made when its value is comparable to the effective objective aperture size. Moreover, a slight interface broadening (≈0.5–1.0 ML) is introduced by the need to orient the interface slightly away from the edge-on condition in order to bring the 002 reflection close to the Bragg condition.[19] Despite these practical concerns, it is significant that the present estimates of interfacial width made using the $\mathbf{g}_{002}$ DFTEM technique are similar to measurements from other materials systems using different methods, such as EELS[19,27] or atom probe tomography.[28,29] For example, a Z-contrast imaging study of interfacial intermixing in InAs/GaSb NCA superlattices indicated interfacial widths (10–90% criterion) of 2.69 and 2.11 ML at InAs-on-GaSb and GaSb-on-InAs interfaces, respectively.[30] An evaluation of InAs/$InAs_{1-x}Sb_x$ superlattices using EELS indicated an intrinsic interface width of L = 1.2 ML (≈1.6 nm using the 10–90% criterion) for the InAsSb-on-InAs interface.[19] Meanwhile, the correspondence between the experimental results of: i) $L_{Cd} = L_{Te}$; ii) little or no interfacial strain (i.e., no change in lattice spacing); and iii) no seemingly

detectable interface features in the HAADF or LABF images, would seem to suggest a well-balanced mixture of II—V and III—VI bonds at the interface rather than preferential formation of III—VI or II—V interfacial compounds. In addition, our work demonstrates the formation of a graded interface extending over 1.5 nm, which agrees with predictions in the literature on the development of mixed interfaces extending over 2–3 atomic layers with minimal electrostatic imbalance.[5,31] Since a perfectly sharp [001] polar interface (charged interface) is highly unstable,[5–7,31] it is anticipated that it will reconstruct into a mixed interface configuration,[5,7] or decompose into individually neutral patches,[31] scenarios that are compatible with our experimental findings. Graded interfaces can encompass different atomic configurations, ranging from a mixed anion plane at the interface, to a mixed cation plane or even intermediate atomic arrangements between these, preserving the charge neutrality condition.[31] The prevalence of In—Te or Cd—Sb bonds at the interface would likely be determined by the presence of a Te and/or Cd overpressure during growth, i.e., by the Cd/Te flux ratio, and, in particular, by the stoichiometry of the surface reconstruction at the growth front.[5] A systematic investigation of the interface properties depending on the growth conditions (surface reconstruction) would now be possible based on the approach described here. Furthermore, the combination of InSb and CdTe to form CdTe/InSb superlattices has been recently proposed.[4,32] The motivation is that built-in electric fields at sharp polar interfaces are predicted to induce a topological transition in the system.[4] However, [001] sharp polar interfaces are very high in energy[4,32] and, consequently, they will likely undergo interfacial atomic exchanges to reduce the energy and become thermodynamically stable. In this respect, our work paves the way to the investigation of the interface configuration at such CdTe/InSb superlattices.

Overall, the method adopted here is of general applicability, and it can be readily applied to other NCA heterovalent interfaces. Hence, the approach opens a new route for investigation of the long-sought correlation between interface-related electronic properties and transport phenomena and the interface characteristics, which would represent a significant advance for implementation of these interfaces in future devices.

4. Experimental Section

The samples under investigation were grown on InSb (001) substrates in a dual-chamber VG V80H MBE system with separate III—V and II—VI chambers connected by an ultrahigh-vacuum (UHV) transfer chamber. First, an InSb buffer layer of 500 nm thickness was grown on the InSb substrate in the III—V chamber. The quality of the InSb buffer was monitored in situ using reflection high-energy electron diffraction (RHEED). The samples were then transferred via a load-lock system to the II—VI chamber under UHV conditions. Immediately prior to CdTe growth, the InSb surfaces were exposed to Cd flux for several minutes to prevent the possible formation of interfacial III—VI compounds. A CdTe buffer layer was then grown using an initial Cd/Te flux ratio of 3.5 in order to further prevent the formation of In_2Te_3 at the interface. After 2 min of growth, the flux ratio was then reduced to 1.5. Upon initiation of the CdTe growth on InSb, the RHEED pattern became slightly hazy as the surface reconstruction transitioned from InSb to CdTe, but after 10 min of growth the pattern became streaky. After growth of a 500 nm thick CdTe buffer layer, $CdTe/Mg_xCd_{1-x}Te$ double heterostructures were grown at a substrate temperature of 265 °C. Further growth details can be found elsewhere.[11] This current work focused specifically on analysis of the CdTe/InSb interface, whereas a detailed investigation reporting growth of the $CdTe/Mg_xCd_{1-x}Te$ double heterostructures was published elsewhere.[17]

One critical step in the (S)TEM investigation of CdTe/InSb-based samples is the TEM specimen preparation. Cross-sectional TEM specimens were prepared for observation in both ⟨110⟩ projections using standard mechanical polishing and dimpling, followed by argon ion milling, typically starting at 2.0 keV and finishing at 0.5 keV. During the ion-milling process, the samples were kept at liquid-nitrogen temperature to minimize any milling-induced artifacts.[33] Chemically sensitive $\mathbf{g}_{002}$ DFTEM imaging was carried out using a JEOL JEM 3010 electron microscope operated at 300 kV and equipped with a GATAN slow-scan charge-coupled-device camera for quantitative image recording. The AC-STEM images were recorded with a JEOL ARM-200F with a HAADF image resolution of ≈0.8 Å when operated in the probe-corrected imaging mode at an accelerating voltage of 200 kV. The beam convergence angle was set at ≈22 mrad, while the collection angles were usually set at 0–22 mrad for (incoherent) LABF imaging, and 90–150 mrad for HAADF imaging. The electron beam direction used for observation was [110] for all the samples.

Acknowledgements

The authors acknowledge use of facilities in the John M. Cowley Center for High Resolution Electron Microscopy at the Arizona State University. The authors also acknowledge assistance from Javier Bartolomé at the initial stages of this work and Bernd Jenichen for critical reading of the manuscript.

Conflict of Interest

The authors declare no conflict of interest.

Keywords

II—VI and III—V semiconductors, (scanning) transmission electron microscopy, CdTe–InSb, interfacial measurements, noncommon-atom heterovalent interfaces

Received: September 27, 2019
Revised: November 29, 2019
Published online: December 17, 2019

[1] R. F. C. Farrow, *J. Vac. Sci. Technol., A* **1985**, *3*, 60.
[2] S. V. Ivanov, V. A. Kaygorodov, S. V. Sorokin, V. A. Solov'ev, A. A. Sitnikova, O. G. Lyublinskaya, Y. V. Terent'ev, Y. B. Vasilyev, V. L. Berkovits, A. A. Toropov, P. S. Kop'ev, *Phys. Status Solidi C* **2004**, *1*, 1468.
[3] A. Franciosi, C. G. Van de Walle, *Surf. Sci. Rep.* **1996**, *25*, 1.
[4] Q. Liu, X. Zhang, L. B. Abdalla, A. Zunger, *Adv. Funct. Mater.* **2016**, *26*, 3259.
[5] H. H. Farrell, M. C. Tamargo, J. L. De Miguel, F. S. Turco, D. M. Hwang, R. E. Nahory, *J. Appl. Phys.* **1991**, *69*, 7021.
[6] A. Kley, J. Neugebauer, *Phys. Rev. B* **1994**, *50*, 8616.
[7] H.-X. Deng, J.-W. Luo, S.-H. Wei, *Phys. Rev. B* **2015**, *91*, 075315.
[8] D. J. Smith, J. Lu, T. Aoki, M. R. McCartney, Y.-H. Zhang, *J. Mater. Res.* **2017**, *32*, 921.

[9] J. M. Burst, J. N. Duenow, D. S. Albin, E. Colegrove, M. O. Reese, J. A. Aguiar, C.-S. Jiang, M. K. Patel, M. M. Al-Jassim, D. Kuciauskas, S. Swain, T. Ablekim, K. G. Lynn, W. K. Metzger, *Nat. Energy* **2016**, *1*, 16015.
[10] Y. Zhao, M. Boccard, S. Liu, J. Becker, X.-H. Zhao, C. M. Campbell, E. Suarez, M. B. Lassise, Z. Holman, Y.-H. Zhang, *Nat. Energy* **2016**, *1*, 16067.
[11] M. J. DiNezza, X.-H. Zhao, S. Liu, A. P. Kirk, Y.-H. Zhang, *Appl. Phys. Lett.* **2013**, *103*, 193901.
[12] D. J. Smith, T. Aoki, J. Mardinly, L. Zhou, M. R. McCartney, *Microscopy* **2013**, *62*, S65.
[13] E. Luna, B. Satpati, J. B. Rodriguez, A. N. Baranov, E. Tournié, A. Trampert, *Appl. Phys. Lett.* **2010**, *96*, 021904.
[14] E. Luna, A. Guzmán, A. Trampert, G. Álvarez, *Phys. Rev. Lett.* **2012**, *109*, 126101.
[15] M. J. Hÿtch, M. G. Walls, J.-P. Chevalier, *Ultramicroscopy* **2000**, *83*, 217.
[16] M. J. Hÿtch, E. Snoeck, R. Kilaas, *Ultramicroscopy* **1998**, *74*, 131.
[17] J. Lu, M. J. DiNezza, X.-H. Zhao, S. Liu, Y.-H. Zhang, A. Kovacs, R. E. Dunin-Borkowski, D. J. Smith, *J. Cryst. Growth* **2016**, *439*, 99.
[18] E. G. Bithell, W. M. Stobbs, *Philos. Mag. A* **1989**, *60*, 39.
[19] J. Lu, E. Luna, T. Aoki, E. H. Steenbergen, Y.-H. Zhang, D. J. Smith, *J. Appl. Phys.* **2016**, *119*, 095702.
[20] E. Luna, F. Ishikawa, B. Satpati, J. B. Rodriguez, E. Tournié, A. Trampert, *J. Cryst. Growth* **2009**, *311*, 1739.
[21] P. A Doyle, P. S. Turner, *Acta Crystallogr., Sect. A: Found. Adv.* **1968**, *24*, 390.
[22] L.-M. Peng, G. Ren, S. L. Dudarev, M. J. Whelan, *Acta Crystallogr., Sect. A: Found. Adv.* **1996**, *52*, 257.
[23] P. A. Stadelmann, JEMS V4, JEMS – SAAS Switzerland, http://www.jems-saas.ch/ (accessed: October 2016).
[24] G. Patriarche, L. Largeau, J. C. Harmand, D. Gollub, *Appl. Phys. Lett.* **2004**, *84*, 203.
[25] G. M. Williams, C. R. Whitehouse, A. G. Cullis, N. G. Chew, G. W. Blackmore, *Appl. Phys. Lett.* **1988**, *53*, 1847.
[26] T. Litz, T. Behr, D. Hommel, A. Waag, G. Landwehr, *J. Appl. Phys.* **1992**, *72*, 3492.
[27] E. Luna, A. M. Beltran, A. M. Sanchez, S. I. Molina, *Appl. Phys. Lett.* **2012**, *101*, 011601.
[28] M. Müller, B. Gault, M. Field, G. J. Sullivan, G. D. W. Smith, C. R. M. Grovenor, *Appl. Phys. Lett.* **2012**, *100*, 083109.
[29] O. Dyck, D. N. Leonard, L. F. Edge, C. A. Jackson, E. J. Pritchett, P. W. Deelman, J. D. Poplawsky, *Adv. Mater. Interfaces* **2017**, *4*, 1700622.
[30] H. Kim, Y. Meng, J.-L. Rouviere, D. Isheim, D. N. Seidman, J.-M. Zuo, *J. Appl. Phys.* **2013**, *113*, 103511.
[31] R. T. Tung, L. Kronik, *Adv. Theory Simul.* **2018**, *1*, 1700001.
[32] H.-X. Deng, B. Huang, S.-H. Wei, *Comput. Mater. Sci.* **2015**, *98*, 340.
[33] C. Wang, D. J. Smith, S. Tobin, T. Parodos, J. Zhao, Y. Chang, S. Sivananthan, *J. Vac. Sci. Technol., A* **2006**, *24*, 995.